Comparative Study of Radiation Mapping Technologies for Nuclear Disaster Assessment

Kotaro Ochi, Evelyne Barker, Shigeo Nakama, Marc Gleizes, Erwan Manach, Vincent Faure, Yukihisa Sanada

https://doi.org/10.20965/jdr.2024.p0429

Paper:

Comparative Study of Radiation Mapping Technologies for Nuclear Disaster Assessment

Kotaro Ochi*,†, Evelyne Barker, Shigeo Nakama*, Marc Gleizes**, Erwan Manach**, Vincent Faure**, and Yukihisa Sanada***

*Collaborative Laboratories for Advanced Decommissioning Science, Japan Atomic Energy Agency
45-169 Sukakeba, Kaihama-aza, Haramachi-ku, Minamisoma, Fukushima 975-0036, Japan
†Corresponding author, E-mail: ochi.kotaro@jaea.go.jp
**Environment Division, Institute for Radiation Protection and Nuclear Safety, Fontenay-aux-Roses, France
[Received July 19, 2023; accepted February 8, 2024]

The distribution of the ambient dose equivalent rate (i.e., air dose rate) after a nuclear disaster is crucial for zoning contaminated areas to facilitate authorities' effective decision making. Several countries are considering a gradual characterization strategy where airborne measurement is performed first followed by ground measurement (i.e., via manborne or carborne surveys). Nonetheless, potential differences might emerge in country-specific air dose rate assessment methods. Explaining these discrepancies can improve and converge existing methodologies. The Japan Atomic Energy Agency (JAEA) and the French Institute for Radiological Protection and Nuclear Safety (IRSN), which are organizations involved in post-nuclear accident crisis management, jointly performed air dose rate measurements in 2019 at contaminated sites around the Fukushima Daiichi Nuclear Power Station. The similarities and differences between the two organizations' methods and results were quantitatively assessed by comparing the average air dose rates obtained within a grid created with a geographic information system, and the reasons for the differences between the organizations' results were investigated. The air dose rates obtained by the manborne measurements varied depending on the calibration method. Comparing the air dose rate assessment methods and mapping techniques used in different countries will contribute to developing international guidelines for recommending the best method for determining air dose rates.

Keywords: Fukushima Daiichi Nuclear Power Station accident, ambient dose equivalent rate, gamma-ray spectrometry, mapping technologies, intercomparison

1. Introduction

After a nuclear power plant accident, one of the most significant objectives is zoning contaminated territories according to the ambient dose equivalent rate (i.e., air dose rate) derived from the radionuclides a reactor releases. The International Atomic Energy Agency (IAEA) has established operational intervention levels to determine zones [1]. Each zone implements protective measures for residents such as evacuation, decontamination, and restrictions on food and drink consumption. Moreover, appropriate monitoring methods should be applied depending on the scale of the identified contaminated area. Several countries are considering a gradual characterization strategy to provide decision makers with information promptly. First, an airborne survey is used to assess the average contamination in the targeted area [2].

In recent years, airborne survey technologies using unmanned aerial vehicles (i.e., drones) have developed remarkably [3–6]. Nonetheless, a complex system response inversion [7] or ground measurement is performed to more precisely delimit contaminated and non-contaminated areas and evaluate the air dose rate near the ground. Mapping can be performed using detectors installed on vehicles and in backpacks carried by humans. Compared with manborne surveys, carborne surveys allow for the rapid assessment of air dose rate distributions over large areas, primarily on roads [8–14]. With a manborne survey, air dose rate distribution can be assessed more locally by moving to areas with high populations [12, 15–18].

In Japan, following the Fukushima Daiichi Nuclear Power Station (FDNPS) accident, instruments and mapping methods for assessing air dose rate distribution have been continuously developed as part of the national mapping project [19]. In particular, the Japan Atomic Energy Agency (JAEA) has conducted airborne surveys using manned helicopters since the FDNPS accident to assess changes in air dose rate distribution in eastern Japan [20]. Moreover, ongoing surveys use unmanned helicopters, which can fly at lower altitudes than manned helicopters, to evaluate the detailed air dose rate distributions within a 5 km radius of the FDNPS [20]. For environments such as urban areas where conducting airborne surveys is challenging, air dose rate distributions have been evaluated using mobile measurements, such as carborne [10] and manborne measurement [16], as well as using measurements taken at fixed points with conventional gamma-ray detectors [21]. In France, which has several operational nuclear power plants, the French Institute for Radiological Protec-

tion and Nuclear Safety (IRSN) plays a central role in characterizing contaminated areas through airborne, carborne, and manborne surveys in case of an accident in a nuclear facility [22].

Although Japan and France have similar overall post-accident contamination characterization strategies, the detectors and data treatment methods used for their airborne, carborne, and manborne surveys might differ, leading to a potential bias in the results. In the event of a nuclear power station accident, radionuclides are dispersed throughout the country where the nuclear power plant is located as well as in neighboring countries [23]. Thus, determining the differences in the responses of the detectors used to assess the dose rates is crucial.

In-situ gamma-ray spectrometry in the field has been documented and published in international guidelines [24, 25]. Thus, aerial measurements have been integrated in different countries and intercomparison exercises have been organized. Examples of international comparisons of air dose rate determination methods include the European Calibration and Coordination of Mobile and Airborne Gamma Spectrometry, which assessed the competence of a manned helicopter and fixed-wing aerial survey teams, primarily in the European project [26–28], and the joint Japanese–Korean cross-check measurements of airborne [29] and ground [12, 30] measurement techniques. However, each study separately discussed airborne and ground measurement techniques for dose rate assessment. Examples of a comprehensive discussion of the two are mainly limited to Japan's measurement techniques [28,31, 32]. Furthermore, the influence of specific conditions on assessing air dose rates and on the measurement results, such as the energy range of interest in the spectrum and the size and type of detectors, has not been assessed.

Comparing different national air dose rate assessment methods allows for the estimation of uncertainty sources in dose rates during nuclear disasters and their impact on the final assessment results. In this study, the JAEA and the IRSN conducted joint manborne, carborne, and airborne surveys in the area surrounding the FDNPS in 2019 to estimate the measurement divergence quantitatively. A comparison of the IRSN's and JAEA's methods can assist in developing international guidelines that recommend the best method for determining air dose rates in the event of future cross-border nuclear disasters.

2. Materials and Methods

2.1. Study Sites

This study was conducted in the Fukushima difficult-to-return zone. The map in **Fig. 1** shows the air dose rates obtained through airborne surveys using manned helicopters that the Nuclear Regulation Authority of Japan conducted between August 29 and September 18, 2019 [32]. The air dose rate data were decay-corrected to September 18, 2019. Using this air dose rate map, manborne and airborne surveys targeted sites with high ^{137}Cs deposition densities [34] and air dose rates that were expected to be significantly higher than the background dose rates [35]. **Fig. 1** shows the locations of the study sites and the survey pathways at each site, and **Table 1** provides basic information about the study sites.

2.2. Materials

A portable gamma-ray spectrometer–dosimeter and a portable dosimeter were employed in the analysis. **Table 2** shows the detectors the JAEA and IRSN used for their surveys.

For the manborne and carborne surveys, the JAEA's and IRSN's portable spectrometers–dosimeters were based on a rectangular CsI(Tl) scintillation detector (1.5 × 1.5 × 1.0 in.) and a cylindrical NaI(Tl) scintillation detector (ϕ3.0 in. × 3.0 in.) associated with Geiger–Müller counters for the IRSN. The multichannel analyzer was adjusted to 1,024 channels, converting the energy range presented in **Table 2**. The gamma-ray spectrum and dose rate are displayed on the tablet. The portable dosemeter the IRSN used comprises a Geiger–Müller counter coupled to a plastic scintillator, covering the energy range presented in **Table 2**. The dose rate and cartography are presented on a tablet. The detector was placed in a backpack and inside the trunk of a car for the manborne and carborne surveys, respectively.

The airborne survey used a portable spectrometer–dosimeter based on three cylindrical $LaBr_3$(Ce) scintillation detectors (ϕ1.5 in. × 1.5 in.) for the JAEA or a semi-cylindrical NaI(Tl) scintillation detector (1.3×2.0 in.) with two Geiger–Müller detectors for the IRSN. The detectors were fixed under the lower part of an unmanned helicopter (Fazer G2, Yamaha Co., Ltd., Japan) used for pesticide application. Each detector was associated with a global navigation satellite system (GNSS) unit to link the air dose rates with location information (**Table 2**). The devices were calibrated in terms of the air dose rate.

2.3. Evaluation of the Air Dose Rates

2.3.1. Evaluation Methods

The gamma-ray interaction with the detector was obtained first to ascertain the counting rate. Conversion of the counting rate into the air dose rate differs according to the equipment used. For some equipment, a conversion factor (CF, [(μSv/h)s]) is calculated from the total counting rate. The counting rate in the energy range (50–7000 keV) is converted to an air does rate when measured with a device using a plastic scintillator as the detector (potable dosimeter) near a ^{137}Cs source. Two methods exist for calculating the CF for equipment with a gamma-ray detector.

The first method for evaluating the CF uses a conversion coefficient ($G(E)$) to represent the contribution of each energy counting rate to the air dose rate [36]. This method can only be applied to gamma-ray spectrometer–dosimeter devices. The $G(E)$ values of the CsI(Tl) and NaI(Tl) scintillation detectors that evaluate dose rates in manborne

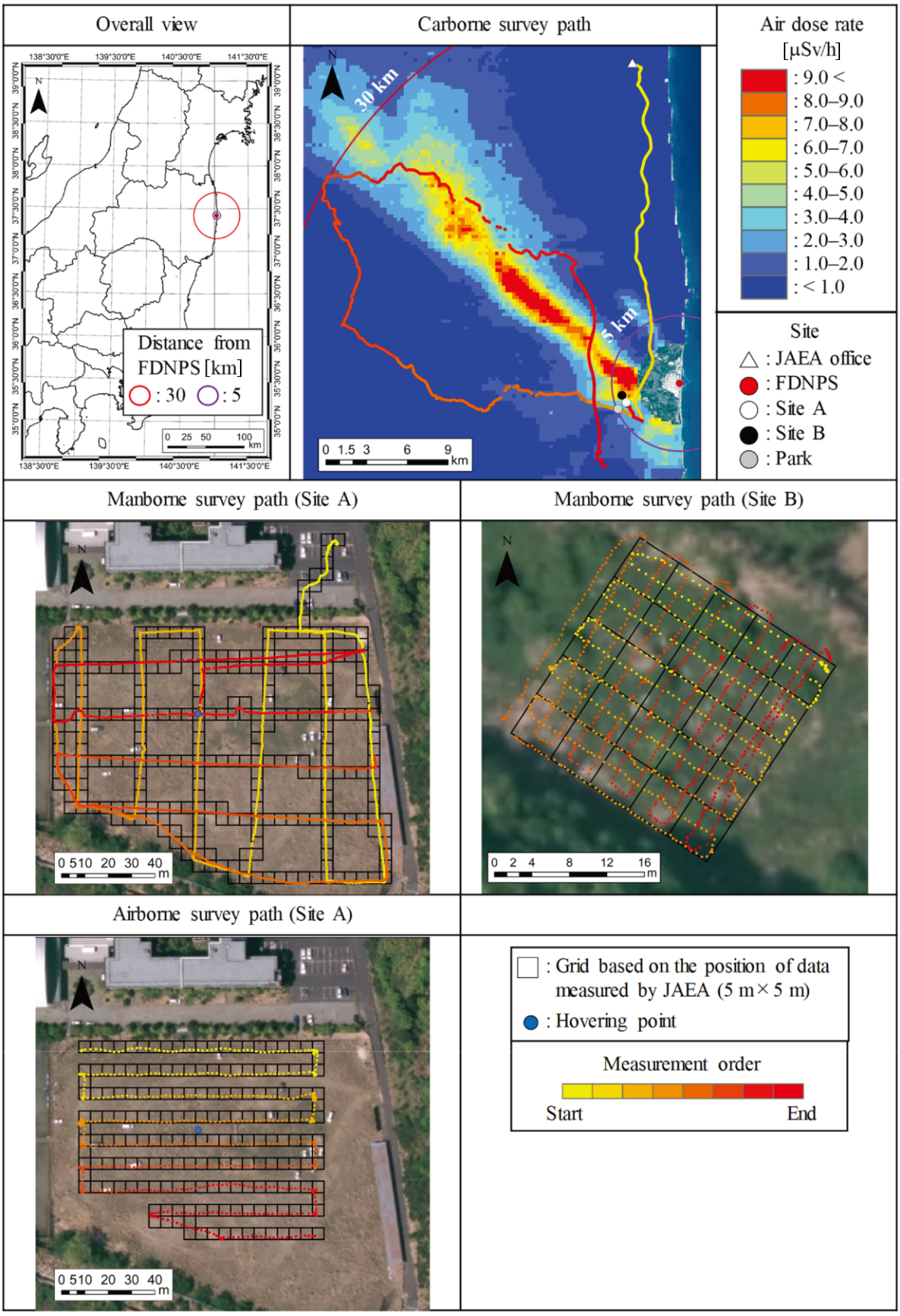

Fig. 1. Site locations and survey paths at each site. This map was created using ArcGIS 10.6.1. The maps of the air dose rate distributions in the top-right image were reconstructed using published data [32]. The background maps in the top-right, middle, and lower images were based on the satellite image taken in April 2018 [33].

Table 1. Basic study site information.

Study site	JAEA office	Site A	Site B	Park
Latitude	37.634520	37.408710	37.413450	37.404390
Longitude	140.994300	140.989300	140.985600	140.982400
Dose rate [μSv/h]	0.0956	3.91	7.81	2.35
Background dose rate [μSv/h]	0.0399	0.0411	0.0423	0.0417
^{137}Cs deposition density [MBq/m^2]	0.0488	2.91	4.46	2.74

Table 2. Information about the devices used in the survey.

Organization	JAEA			IRSN		
Survey	Manborne	Carborne	Airborne	Manborne	Manborne and carborne	Airborne
Image			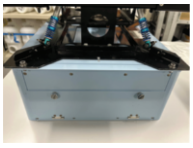			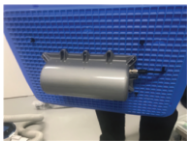
Manufacturer (detector)	Hamamatsu Photonics Co., Ltd.		Japan Radiation Engineering Co., Ltd.	Saphymo	Mirion Technologies Inc.	
Element (crystal)	CsI(Tl) (1.5 × 1.5 × 1.0 in.)		$LaBr_3$(Ce) (ϕ1.5 in. × 1.5 in. × 3)	Plastic scintillator	NaI(Tl) (ϕ3.0 in. × 3.0 in. or 1.3 × 2.0 in.) and two Geiger–Müller counters	
ROI [keV]	30–2000		50–2800	50–7000	30–3000	
Time constant [μs]	12		7.0	–	–	–
Integration interval of counts [s]	1.0		1.0	1.0	1.0	
Manufacturer (GNSS)	Hemisphere Co., Ltd.		NovAtel Inc.	GENEQ Inc.	EOS Positioning Systems	
Model	A325 GNSS Smart Antenna		OEM 729	SXBlue	ARROW	
Received signal	GPS, GLONASS		GPS, GLONASS, Galileo, etc.	GPS, GLONASS	GPS, GLONASS, Galileo, BeiDou	
Positioning system	Differential					
CF_{all} [(μSv/h)s] (Site A)	4.51×10^{-4}	4.51×10^{-4}	2.55×10^{-4}	–	1.11×10^{-4}	8.32×10^{-4}

and carborne surveys were calculated using Monte Carlo simulations. **Fig. 2** shows an example of $G(E)$ for the CsI(Tl) scintillation detector. The air dose rates obtained from manborne and carborne surveys are estimated from Eq. (1):

$$D = \int_{E_{min}}^{E_{max}} G(E)N(E)\,dE, \quad \ldots\ldots\ldots \quad (1)$$

where D is the air dose rate [μSv/h], $E_{max/min}$ are the maximum and minimum values of the gamma-ray energy on the spectrum in the limited energy range [keV], $G(E)$ is the conversion coefficient [(μSv/h)s], and $N(E)$ is the counting rate at energy E [/s/keV].

The second method for evaluating CF uses CF_{all}, which considers the counting rate integrated over an energy range [20]. In this study's manborne and carborne surveys, air dose rates were evaluated using the first method. However, to facilitate comparison with CF_{all} used in the airborne surveys, CF_{all} for manborne and carborne surveys was determined by considering either the air dose rate calculated using the second method outside the car during the carborne survey or by taking the air dose rate values from

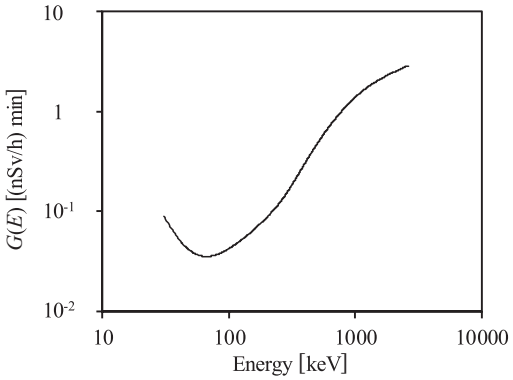

Fig. 2. Pulse height of air dose rate conversion function $G(E)$ for a CsI(Tl) scintillation detector.

a reference handle radiometer (**Table 2**). For the airborne survey, CF_{all} was obtained using the geometric mean of the air dose rates obtained via manborne survey within a radius of 30 m from the hovering point and the counting rate obtained at 1 m above ground level (agl.) via the air-

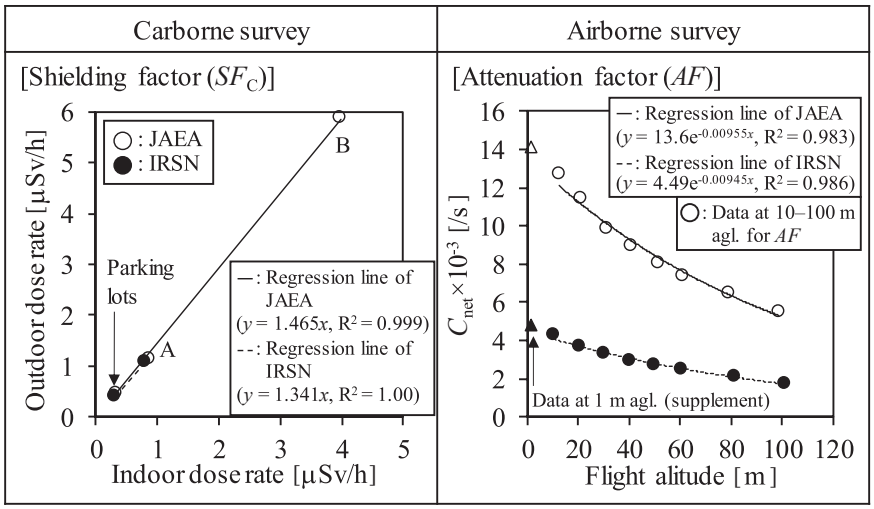

Fig. 3. Evaluation result of shielding and attenuation factors.

borne survey at the same point. The JAEA and the IRSN focused on counting rates of 50–2800 and 30–3000 keV, respectively, to avoid the influence of cosmic rays (**Table 2**). The equations for the air dose rates obtained via airborne survey are described in Section 2.3.3.

The choice between the first and second methods depends on the composition of the radionuclides deposited on the target ground surface. Approximately one month after an accident, most short-lived nuclides, such as ^{131}I and ^{133}Xe, have decayed, leaving radiocesium (^{134}Cs and ^{137}Cs) in the environment as the primary radionuclide [37]. Applying the CF_{all} method based on the counting rate integrated over an energy range is preferable in an environment with few radionuclide types at a specific time after the fallout.

2.3.2. Attenuation Carrier Correction

Except for airborne measurements where the gamma-ray flux from the ground directly arrives at the detector surface, radiation attenuation due to the human body or a car must be considered in manborne and carborne surveys. The attenuation corrective factor (SF_H and SF_C for a human body or a car, respectively) is determined by measuring the gamma-ray flux with and without the carrier. Since the car used for the carborne survey was not the typical model the IRSN uses, the air dose rates were measured at several sites (sites A and B and parking lots) inside and outside the vehicle while staying at the same location to calculate SF_C. The slope of the linear correlation equation represents the relationship between the dose rates inside and outside the car, corresponding to the SF_C (**Fig. 3**).

2.3.3. Attenuation Air Correction and a Method for Calculating the Air Dose Rate at 1 m agl.

The counting rate attenuates exponentially with increasing altitude (**Fig. 3**), necessitating conversion of the air dose rate measured by airborne survey into a dose rate at 1 m agl., which represents the impact on the population. For airborne surveys, the IRSN calculates air dose rates using two methods. The first method, the IRSN method, is implemented through data acquisition software using Eq. (2) to calculate air dose rates at 1 m agl. [25, 38].

$$D_{1m} = D_L + D_{Cos} + D_{Rad} + D_{BG}, \quad \ldots\ldots \quad (2)$$

where D_L is the local air dose rate based on $G(E)$ in Eq. (1) without a natural dose rate contribution calculated at 1 m agl. [μSv/h], D_{Cos} is the air dose rate derived from the cosmic rays at 1 m agl. [μSv/h], D_{Rad} is the air dose rate derived from the radon progeny at 1 m agl. [μSv/h], and D_{BG} is the background air dose rate derived from self-contamination of the detector [μSv/h]. The detailed calculation methods for each dose rate are shown in Eqs. (5)–(10).

The second method, the JAEA method, is based on Eq. (3) [20].

$$D_{1m} = (C_{all} - C_{BG}) CF_{all} \exp\left[-AF(H_m - H_{std})\right], \quad (3)$$

where C_{all} is the total counting rate [/s] at 50–2800 or 30–3000 keV, C_{BG} is the background counting rate, including self-contamination of the detector [/s], AF is the attenuation factor [/m], H_m is the flight altitude agl. [m], and H_{std} is the standard altitude agl. (1 m).

Unmanned helicopter flights at 10–100 m in hover mode were used to estimate AF at site A. The same altitude was maintained for at least 100 s. The average C_{all} at different altitudes was determined. The slope of the exponential formulation of the average net counting rate (C_{net}) at 10–100 m agl. was used to obtain the AF (**Fig. 3**).

Since the $LaBr_3$(Ce) detectors the JAEA uses contain ^{138}La, a radioactive element, self-contamination of the detector must be evaluated. Background spectra were collected by aircraft hovering at 200 m offshore of the Ukedo River to analyze the average C_{BG}. The counting rates of C_{all} and C_{BG} were integrated over the energy range (**Table 2**). However, the NaI(Tl) scintillation detector the IRSN uses has lower self-contamination than $LaBr_3$(Ce)

Table 3. Basic information about the surveys.

Survey	Manborne		Carborne	Airborne
Site	A	B	Road between sites	A
Survey date	Nov. 6, 2019	Nov. 7, 2019	Nov. 7, 2019	Nov. 1, 2019 (JAEA) Nov. 7, 2019 (IRSN)
Survey condition	Grid pattern		Line pattern	Line pattern hovering
Movement speed [m/s]	0.5		16	2.0
Survey line interval [m]	2.5	25	–	10

detectors. The IRSN performed a hover flight at 50 m agl. at a non-contaminated site and over the sea to determine the NaI(Tl) scintillation detector's C_{BG}.

2.4. Measurement Strategy for the Intercomparison

Both organizations performed each survey on the same day or week for the airborne measurement to directly compare the results. For the manborne survey, the JAEA and IRSN measurements were taken by walking along the same route. For the carborne survey, both organizations' detectors were placed in the trunk of the same car at 1 m agl. For the airborne survey, both organizations' detectors were mounted on the same unmanned helicopter with the program set to allow them to measure the same route at the same speed and altitude at site A.

For each site, the measurement parameters were previously defined, including the characterization pattern (line and grid), the distance between the lines, and the speed. **Table 3** summarizes these measurement conditions.

2.5. Air Dose Rate Intercomparison Method

The average air dose rates obtained by the JAEA and the IRSN within a common grid were compared using Eq. (4):

$$\text{Relative deviation (RD)} = \frac{D_{\text{I}} - D_{\text{J}}}{D_{\text{J}}}, \quad \ldots \quad (4)$$

where D_{I} and D_{J} are the air dose rates obtained by the IRSN and the JAEA [μSv/h], respectively. A detailed schematic of the creation of a common grid is provided in Appendix A. The closer the median and mean of the RD are to zero, the lower the difference between the air dose rates measured by the two organizations.

3. Results and Discussion

3.1. Conversion Factors for Air Dose Rates

For the manborne and carborne surveys, conversion of the counting rate to the air dose rate was based on Eq. (1). For the airborne survey, CF_{all} used in Eq. (3) is presented in **Table 2**. The $LaBr_3$(Ce) detector the JAEA used in the airborne survey had three scintillators with a higher detection surface than the NaI(Tl) detector of the IRSN. Thus, the CF_{all} in the airborne survey was lower than that in the other survey. The CF_{all} values used in Eq. (3) for the manborne and carborne surveys were compared (**Table 2**). **Fig. 4** shows the distributions of CF_{all} at the three sites. The between-site differences in the mean values of CF_{all} can be ascribed to differences in the composition of the radionuclides deposited on the ground surface, that is, the Compton scattering contribution of radionuclides. **Fig. 5** presents examples of the gamma-ray spectra obtained at different sites, where the intensities of the full absorption peaks of each radionuclide varied significantly in areas with different air dose rates.

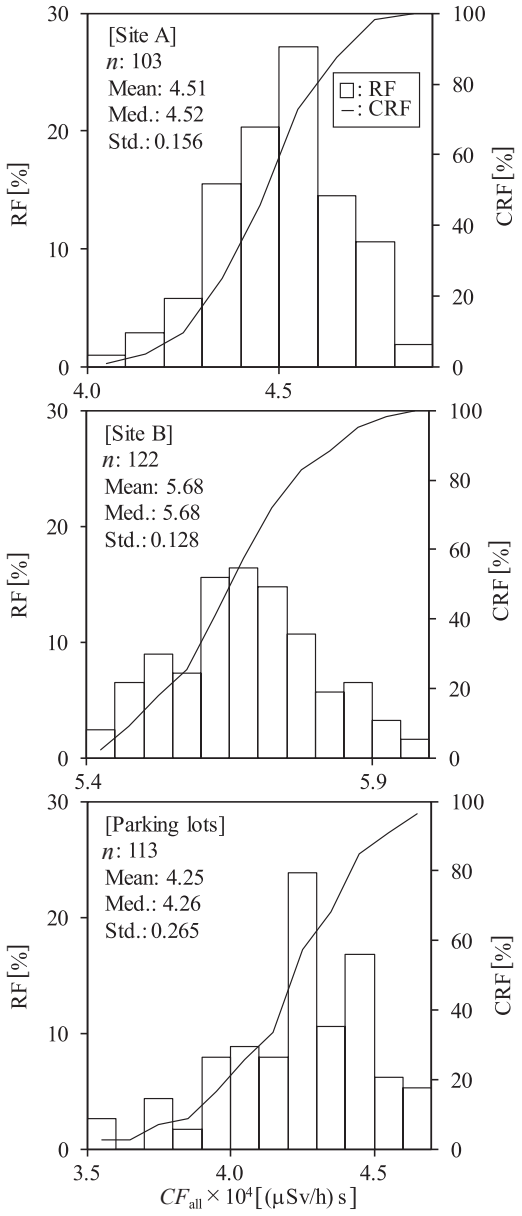

Fig. 4. Distribution of CF_{all} for the manborne survey obtained using the JAEA's detector. RF: relative frequency; CRF: cumulative relative frequency.

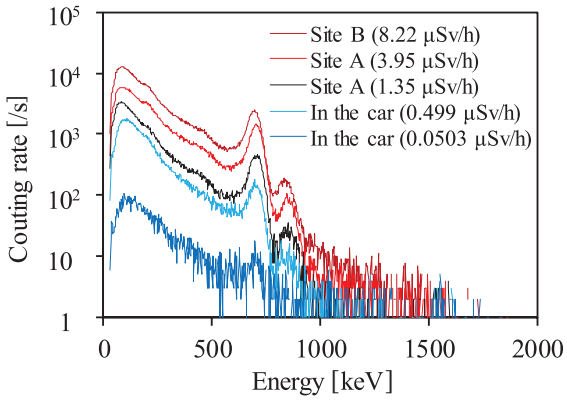

Fig. 5. Gamma-ray spectra measured with a CsI(Tl) scintillation detector for 2 min. obtained by the manborne survey.

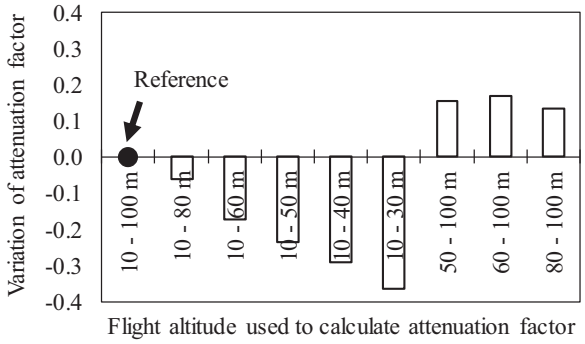

Fig. 6. Variations in attenuation factor with flight altitude during evaluation.

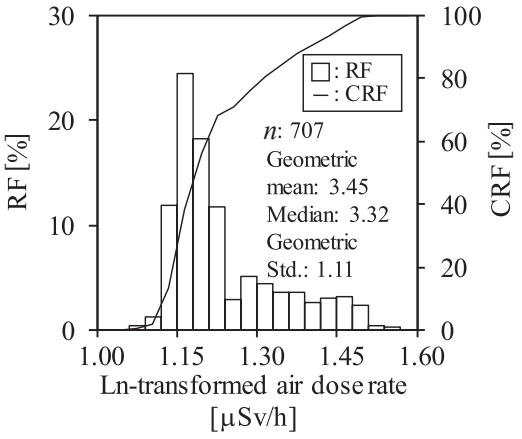

Fig. 7. Distribution of the ln-transformed air dose rates obtained by the manborne survey at site A (JAEA). RF: relative frequency; CRF: cumulative relative frequency.

3.2. Corrective Factor

The air dose rate should be precise when evaluating site contamination. In a manborne survey, the attenuation of gamma-rays by a carrier (SF_H) along the way of the gamma-ray flux to the detector must be considered. Given that the radionuclides remaining at sites A and B were Cs isotopes (**Fig. 5**), the IRSN used a correction factor of 1.23 based on the human body's gamma-ray shielding (the mean value for Cs isotopes is from Ref. [39, 40] for 3 in. detectors and personal communication (not published)). For the JAEA, the air dose rates were measured and compared using a CsI(Tl) scintillation detector and ϕ1.0 in. ×1.0 in. NaI(Tl) scintillation detector (TCS-172B, Hitachi-Aloka Ltd., Tokyo, Japan) at various points in a previous study [12, 30]. Moreover, the JAEA used a correction factor of 1.40 to address the human body's gamma-ray shielding.

Figure 3 shows the average air dose rates measured inside and outside the car at three sites (sites A, B, and nearby parking lots) for calculating the SF_C used for the carborne survey. This study showed that the bias due to the methods used to determine the SF_C was approximately 10%. The same SF_C value was used to explain the differences between the characteristics of the JAEA's and IRSN's detectors and the similar air dose rates inside the car. Determining SF_C for the airborne survey was unnecessary because the detector was below the unmanned helicopter.

3.3. Air Dose Rate Calculation at 1 m agl.

For the manborne and carborne surveys, the measurement height was approximately 1 m agl., different from the airborne measurements. The dose rate in the airborne survey at a flight altitude of 1 m agl. was converted using Eq. (3). The relationship between the mean value of C_{net} and the ground altitude is shown in **Fig. 3** to calculate the AF using Eq. (3). The counting rate the IRSN measured was statistically lower than that measured by the JAEA (Welch's t-test, $^*p < 0.05$). This result reflects the difference in the total detection volume used by the two organizations. Nonetheless, the AF uncertainty was considered small based on the variations in the C_{net} the JAEA measured when the altitude was less than 2%. Due to the IRSN detector's small volume, the total absorption peak of radiocesium (approximately 605 keV and 662 keV) on the gamma-ray spectrum measured 40 m agl. at the contaminated site with an air dose rate of 3–4 μSv/h, which was not clearly distinguished from the spectrum baseline. The AF variations according to the flight levels were investigated to evaluate the AF factor with a bias of up to 35% for the IRSN detector (**Fig. 6**); however, the impact on the air dose rate determination was 1%–11%.

The C_{net} at 1 m agl. calculated by extrapolating the exponential relation in **Fig. 3** and C_{net} measured at 1 m agl. in the supplementary data correlated well. Therefore, the counting rate based on hovering flights could reasonably evaluate CF_{all}. Furthermore, a measurement with an unmanned aerial detector at 1 m agl. was unnecessary.

Expressing the air dose rate measured at a flight altitude of several meters to an air dose rate at 1 m agl. is subject to the assumption of homogeneity of contamination in the detector's field of view. **Fig. 7** visualizes a histogram of the ln-transformed air dose rates from the manborne survey within a radius of 30 m from the hovering point,

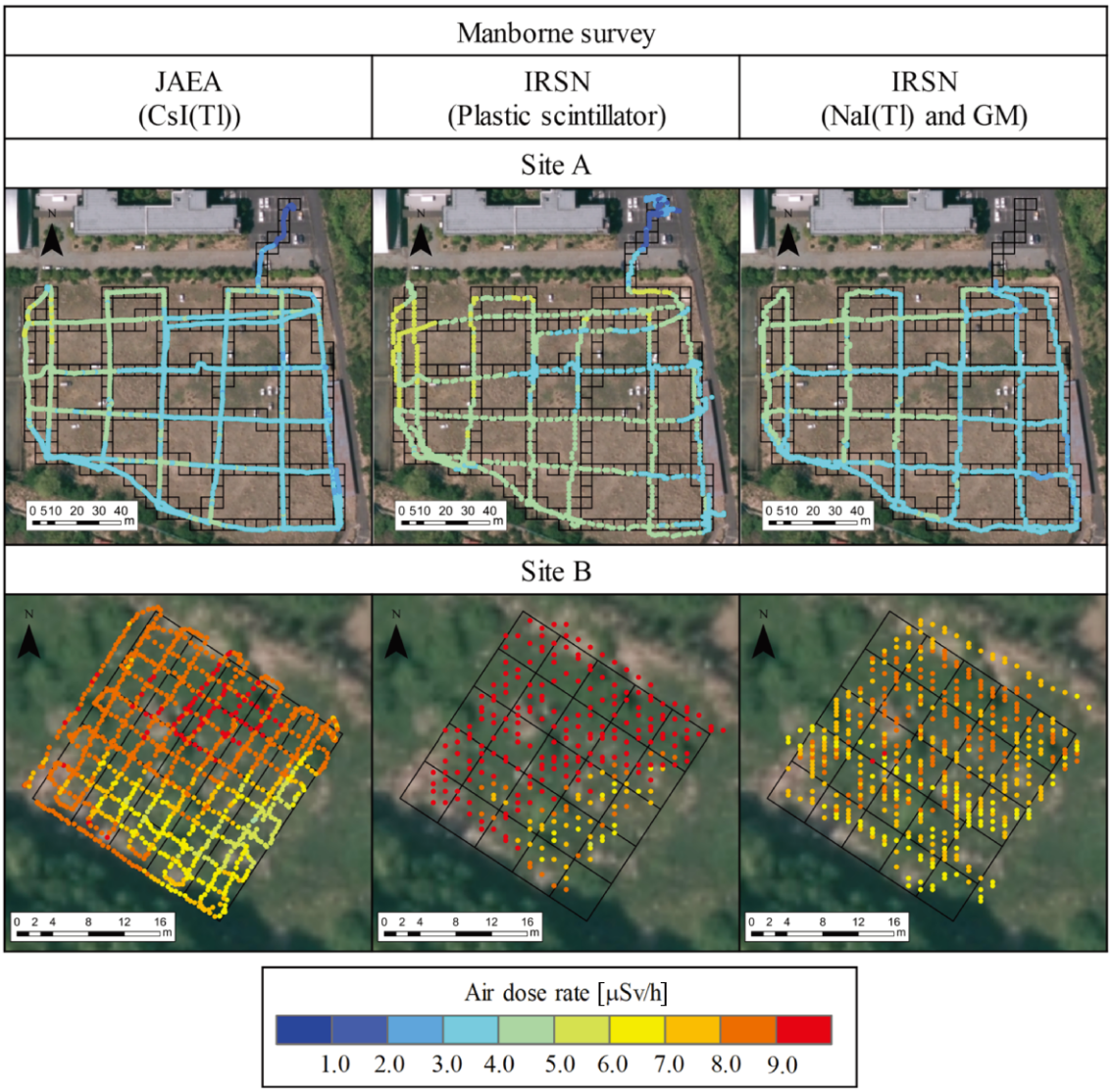

Fig. 8. Distribution of the air dose rates at 1 m agl. obtained by manborne surveys at sites A and B. This map was created using ArcGIS 10.6.1.

showing a non-log normal distribution reflecting heterogeneous ground contamination. Thus, the CF_{all} determination used the mean value of the manborne survey at a radius of 30 m around a hovering point. The contribution of radiocesium-derived gamma-rays deposited in an area within a radius of 30 m to the air dose rate at an altitude of 20 m is approximately 30% [2]. Therefore, the gamma-rays can be ascribed to an area wider than the area range on which this study focused, resulting in a discrepancy between the airborne and manborne survey results. Nonetheless, it was considered a more reasonable representation of the actual air dose rate distribution on the ground surface than the dose rate value directly obtained below the hovering point. Considering the small uncertainty of AF in evaluating CF_{all} in the airborne survey and the geometric standard deviation of the air dose rates shown in **Fig. 7**, the heterogeneity of the air dose rates at the ground surface within an area was considered the primary contributor to the uncertainty in evaluating CF_{all} for the airborne survey.

3.4. Distribution of Air Dose Rates

Manborne surveys were conducted at sites A and B (**Fig. 8**). Both organizations' measurements revealed the non-uniform distribution of air dose rates in the area. **Fig. 9** shows the air dose rate distributions obtained from the carborne survey. The characterizations highlighted the validity of the manborne survey as a suitable for local-scale zoning, whereas the carborne survey was deemed as a suitable method for the rapid zoning of large areas accessible by road. **Fig. 10** shows the air dose rate distributions obtained from the airborne survey at site A, confirming that the airborne survey is the best method for assessing the air dose rate distribution over a wide area.

Several biases in the air dose rate distributions were observed, especially for the manborne survey at site B and the airborne survey at site A. The primary reason for the discrepancy between the air dose rate distributions the JAEA and the IRSN measured is the accuracy of the GNSS unit the IRSN used. For site B, although both organizations

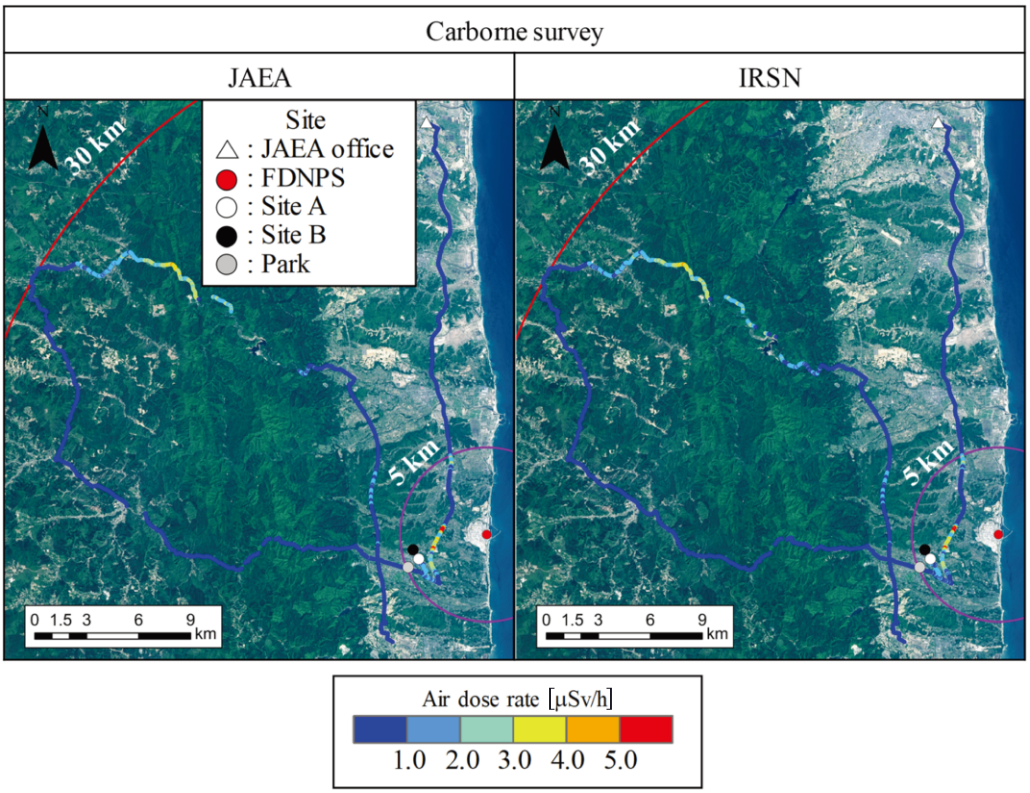

Fig. 9. Distribution of air dose rates at 1 m agl. obtained by carborne survey. This map was created using ArcGIS 10.6.1.

followed the same route (grid pattern), the trajectory of the IRSN measurements deviated from that of the JAEA in some areas by several meters. Similarly, for the airborne survey, the IRSN measurements deviated by several meters in the southeast direction relative to the JAEA results. The most northerly measurement lines were off when measured by the IRSN at an altitude of 10 m agl. because nearby schools shielded the radio waves the satellite emitted at lower altitudes. The higher the flight altitude, the closer the IRSN's flight trajectory approached that of the JAEA, validating this hypothesis. This deviation resulted from the limited accuracy of the GNSS unit the IRSN used, which could be improved by increasing the sensitivity of the receiver for countries outside the European zone.

3.5. Intercomparison Results

Figure 11 shows the RD histogram of air dose rates and correlations to quantitatively evaluate the divergence of the air dose rates the two organizations measured. For the manborne, carborne, and airborne surveys, the air dose rates the IRSN measured were 0.5–2.0 times those measured by the JAEA.

For the manborne survey, the air dose rates the IRSN measured with the plastic scintillation detector differed significantly from those the JAEA measured with the CsI(Tl) scintillation detector (Welch's t-test, $^*p < 0.05$), with the average RD indicating that the former was approximately 16% higher than the latter. No statistical difference occurred between the air dose rates the JAEA measured with CsI(Tl) and those the IRSN measured with the NaI(Tl) scintillation detector (Student's t-test, $^*p \geqq 0.05$) because of the detectors' similar dose rate calculation methods. The plastic scintillator the IRSN used focused on the counting rate derived from gamma- and beta-rays and on an energy range wider than that of the CsI(Tl) or NaI(Tl) detectors. However, considering the shielding of the beta-rays by the electrical components, the backpack around the detector, and the body of the person carrying the backpack, most of the contribution to the air dose rate can be ascribed to the gamma-rays emitting from radionuclides. In the manborne and airborne surveys, the data outside the targeted grid were excluded from the analysis due to the GNSS equipment's performance limitations.

Comparison of the data between the manborne and airborne surveys (**Fig. 12**) did not exhibit significant differences between the air dose rates obtained from the IRSN airborne surveys using the JAEA method at an altitude of 10 m and those obtained from the JAEA manborne survey (Welch's t-test, $^*p \geqq 0.05$). Significant differences were found between the two at other flight altitudes (Welch's t-test, $^*p < 0.05$). The mean and median RDs deviated from zero at higher altitudes in both organizations' results, with a greater deviation being observed for the JAEA airborne survey. This discrepancy indicates differences in the measurement characteristics of the JAEA's and IRSN's detectors when assessing heterogeneous ground contamination [2, 32].

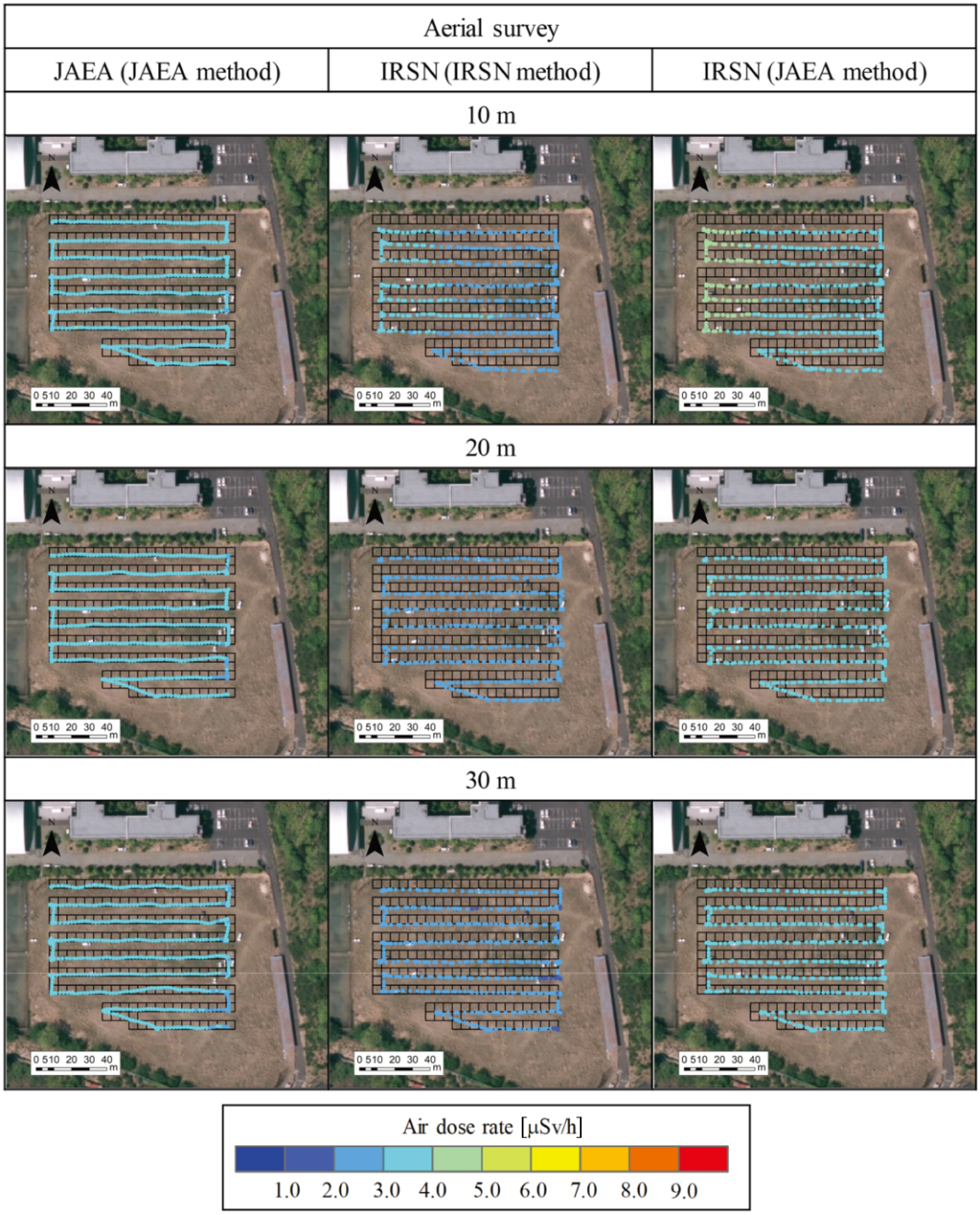

Fig. 10. Distribution of air dose rates at 1 m agl. obtained by airborne survey in site A. This map was created using ArcGIS 10.6.1.

4. Conclusions

Although no standard measurement methods exist for post-nuclear disaster assessment of contaminated areas, some countries, such as Japan and France, have the same strategy using similar equipment, that is, a preliminary characterization phase using a manned helicopter, followed by improving the results obtained in the contaminated and uncontaminated areas using an unmanned helicopter at a low altitude and manborne surveys. Carborne surveys supplement these characterizations for areas accessible by car.

The JAEA and IRSN conducted joint manborne, carborne, and airborne surveys around the FDNPS in this study. This opportunity to realize such joint measurements in "peacetime" allows for the exchange of post-accident measurement strategies. This opportunity also permits comparison of data treatment methods and determination of uncertainties, which are crucial for cross-border evaluation of contaminated zones in the case of nuclear disasters. The following findings were obtained.

1. The manborne survey results showed that the air dose rates the IRSN measured were similar to those measured by the JAEA based on comparison of the data obtained by the NaI(Tl) and CsI(Tl) detectors given that the same evaluation method was used. A plas-

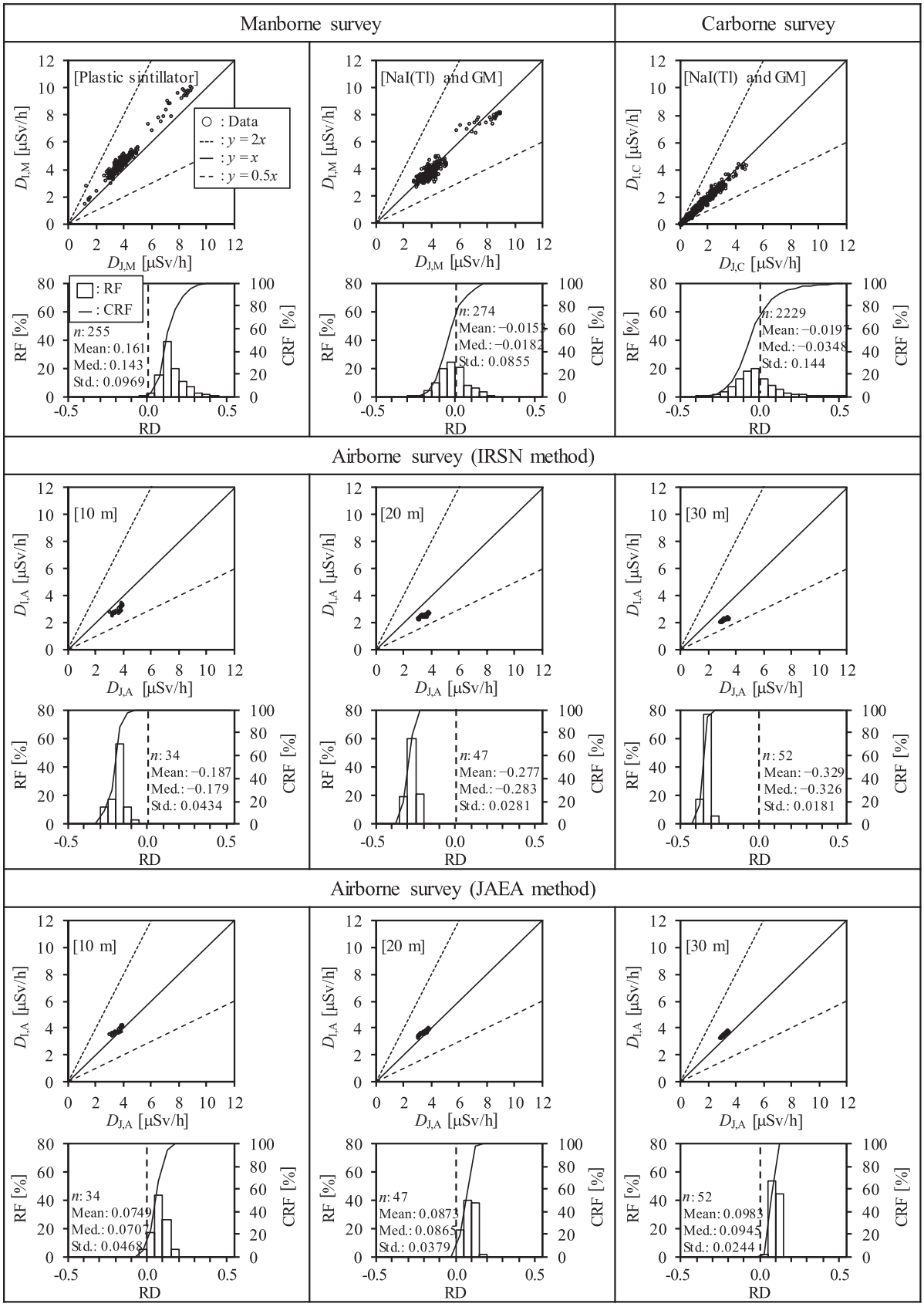

Fig. 11. Intercomparison result of air dose rates obtained by JAEA and IRSN. D_I, D_J, D_M, D_C, and D_A indicate air dose rates obtained by IRSN, JAEA, manborne survey, carborne survey, and airborne survey, respectively. RD: relative deviation; RF: relative frequency; CRF: cumulative relative frequency.

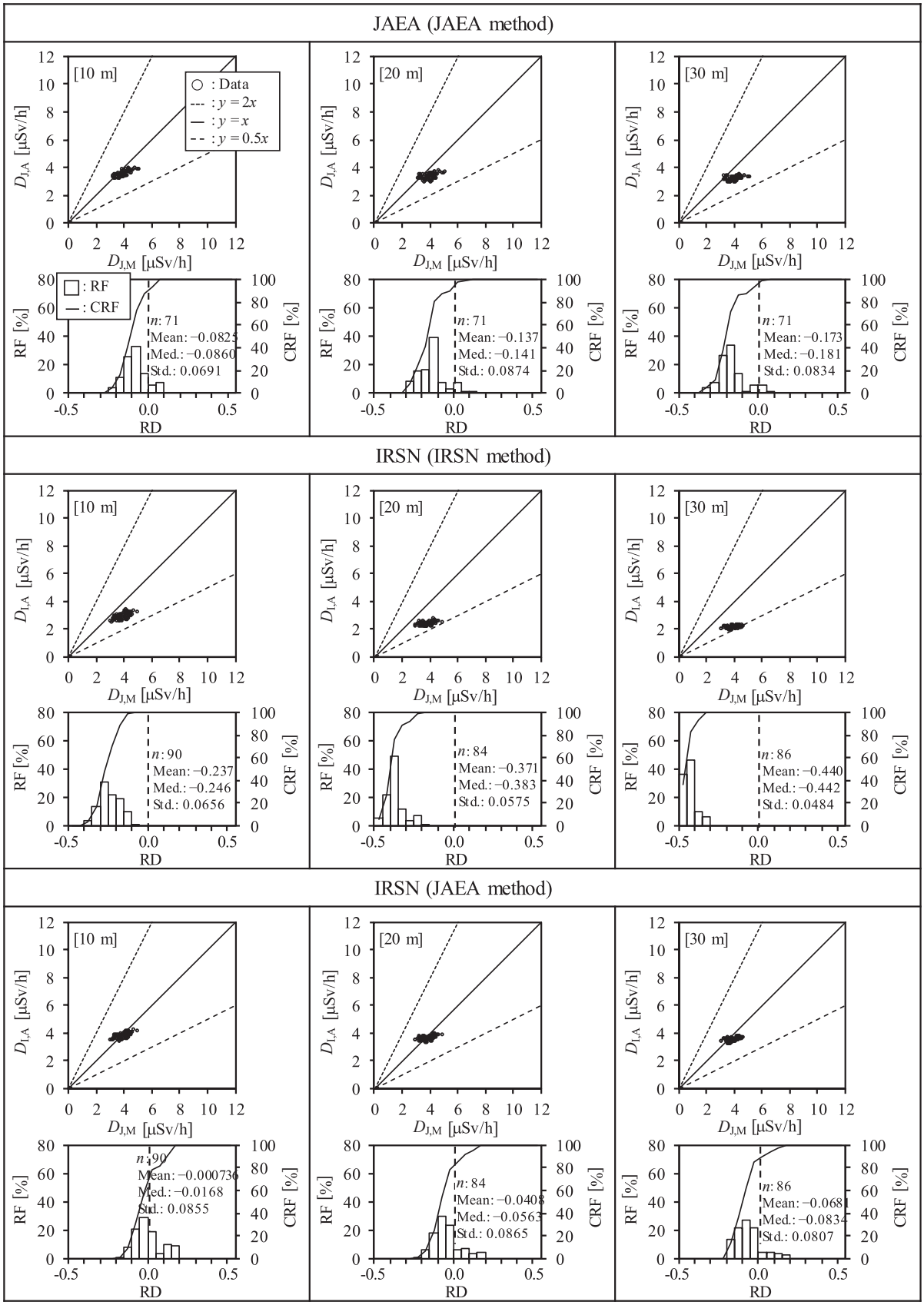

Fig. 12. Intercomparison result of the air dose rates obtained by the manborne and airborne surveys. D_{I}, D_{J}, D_{M}, D_{C}, and D_{A} indicate air dose rates obtained by IRSN, JAEA, manborne survey, carborne survey, and airborne survey, respectively. RD: relative deviation; RF: relative frequency; CRF: cumulative relative frequency.

tic scintillation detector yields higher air dose rates (16%) because of the process used to convert the count rate to estimate the air dose rate.

2. The carborne survey results confirmed that the air dose rates the two organizations measured correlated well. The method used to calculate the car attenuation to obtain an air dose rate in the environment and not in the car could lead to a difference of approximately 10%.

3. The airborne survey results showed that the air dose rates evaluated with the same methodology (the JAEA method) presented smaller differences between the organizations with less than 10% bias. This intercomparison highlighted the need for all organizations to use the same data processing method to calculate the air dose rate at 1 m agl.

4. For the airborne survey, *AF*, one of the parameters needed to convert the air dose rate at flight altitude into a height of 1 m agl., was determined by hovering at a ground altitude of 10–100 m. *AF* assessment at smaller altitudes had a lower impact on the air dose rate (in the range of 1%–11%).

5. In particular, the GNSS units' reception accuracy was expected to affect the grid comparison method results.

6. The discrepancy in the air dose rates between manborne and airborne surveys became significant as the ground altitude increased under heterogeneous contamination.

These results confirmed the effectiveness of both organizations' post-nuclear accident radiological monitoring methods. Since each organization has its own monitoring methods, continuous cooperation can enable rapid sharing of information on the diffusion of radioactive materials and the associated distribution of air dose rates in the event of a nuclear power plant accident or similar emergencies.

Acknowledgments

We gratefully acknowledge the valuable help we received from the staff of the Fukushima Environmental Evaluation Research Division in the JAEA, Japan Radiation Engineering Co., Ltd., JDRONE Co., Ltd., and Clear Pulse Co., Ltd. Conflict of Interest: The authors declare that they have no conflicts of interest. Funding: This study was funded by the Nuclear Regulation Authority, Japan.

References:

[1] International Atomic Energy Agency, "Operational Intervention Levels for Reactor Emergencies and Methodology for Their Derivation, Emergency Preparedness and Response," IAEA, 2017. https://www.iaea.org/publications/11093/operational-intervention-levels-for-reactor-emergencies [Accessed March 12, 2024]

[2] A. Malins, M. Okumura, M. Machida, H. Takemiya, and K. Saito, "Fields of view for environmental radioactivity," Proc. of the 2015 Int. Symp. on Radiological Issues for Fukushima's Revitalized Future, pp. 28-34, 2015.

[3] M. Lowdon, P. G. Marin, M. W. J. Hubbrad, M. P. Taggart, D. T. Connor, Y. Verbelen, P. J. Sellin, and T. B. Scott, "Evaluation of Scintillator Detection Materials for Application within Airborne Environmental Radiation Monitoring," Sensors, Vol.19, No.18, Article No.3828, 2019. https://doi.org/10.3390/s19183828

[4] C. M. Chen, L. E. Sinclair, R. Fortin, M. Coyle, and C. Samson, "In-Flight Performance of the Advanced Radiation Detector for UAV Operations (ARDUO)," Nucl. Inst. Metho. Phys. Res. A, Vol.954, Article No.161609, 2020. https://doi.org/10.1016/j.nima.2018.11.068

[5] A. Vargas, D. Costa, M. Macias, P. Royo, E. Pastor, M. Luchkov, S. Neumaier, U. Stöhlker, and R. Luff, "Comparison of airborne radiation detectors carried by rotary-wing unmanned aerial systems." Rad. Meas., Vol.145, Article No.106595, 2021. https://doi.org/10.1016/j.radmeas.2021.106595

[6] X. Jia, G. Qin, F. Li, and G. Zhao, "Design of an Airborne γ-ray Spectrometry System Based on Unmanned Aerial Vehicle," J. Phys., Vol.2449, Article No.012043, 2023. https://doi.org/10.1088/1742-6596/2449/1/012043

[7] L. E. Sinclair and R. Fortin, "Spatial deconvolution of aerial radiometric survey and its application to the fallout from a rediological dispersal device," J. Environ. Radioact., Vol.197, pp. 39-47, 2019. https://doi.org/10.1016/j.jenvrad.2018.10.014

[8] T. Furutani, K. Uehara, and J. Murai, "A Study on Comminity-Based Reconstruction from Nuclear Power Plant Disaster – A Case Study of Minamisoma Ota Area in Fukushima –," J. Disaster Res., Vol.7, No.sp, pp. 432-438, 2012. https://doi.org/10.20965/jdr.2012.p0432

[9] N. M. Hassan, Y. J. Kim, J. Jang, B. U. Chang, and J. S. Chae, "Comparative study of precise measurements of natural radionuclides and radiation dose using *in-situ* and laboratory γ-ray spectroscopy techniques," Sci. Rep., Vol.8, Article No.14115, 2018. https://doi.org/10.1038/s41598-018-32220-9

[10] M. Andoh, S. Mikami, S. Tsuda, T. Yoshida, N. Matsuda, and K. Saito, "Decreasing trend of ambient does equivalent rates over a wide area in eastern Japan until 2016 evaluated by carborne surveys using KURAMA systems," J. Environ. Radioact., Vol.210, Article No.105813, 2019. https://doi.org/10.1016/j.jenvrad.2018.09.011

[11] E. Prieto, E. Jabaloyas, R. Gasanovas, C. Rovira, and M. Salvadó, "Set up of a gamma spectrometry mobile unit equipped with $LaBr_3$(Ce) detectors for radioactivity monitoring," Rad. Phys. Chem., Vol.168, Article No.108600, 2020. https://doi.org/10.1016/j.radphyschem.2019.108600

[12] Y.-Y. Ji, K. Ochi, S. B. Hong, S. Nakama, Y. Sanada, and S. Mikami, "Joint Environmental Radiation Survey by JAEA and KAERI Around the Fukushima Daiichi Nuclear Power Plant: Performance of Mobile Gamma-Ray Spectrometry Using Backpack and Carborne Survey Platforms," Health Phys., Vol.121, No.6, pp. 613-620, 2021. https://doi.org/10.1097/HP.0000000000001471

[13] R. Pradana, E. D. Nugraha, W. Wahyudi, U. Untara, M. Wiyono, A. Devriany, S. N. Shilfa, M. Sasaki, H. Prasetio, I. D. Winarni, E. Ekaranti, N. Nuraeni, C. Kranrod, D. Iskandar, G. Suhariyono, H. N. E. Surniyantoro, M. Makhsun, S. Widodo, Y. Omori, E. Hiswara, M. Hosoda, S. Yoshinaga, and S. Tokonami, "Carborne survey and dose assessment from external radiation exposure in Bangka Island," Environ. Sci. Pollut. Res., Vol.30, pp. 89280-89292, 2023. https://doi.org/10.1007/s11356-023-28640-4

[14] F. S. Russel-Pavier, S. Kaluvan, D. Megson-Smith, D. T. Corner, S. J. Fearn, E. L. Connolly, T. B. Scott, and P. G. Martin, "A highly scalable and autonomous spectroscopic radiation mapping system with resilient IoT detector units for dosimetry, safety and security," J. Radiol. Port., Vol.43, Article No.011503, 2023. https://doi.org/10.1088/1361-6498/acab0b

[15] A. J. Cresswell, D. C. W. Sanderson, M. Harrold, B. Kirley, C. Mitchell, and A. Weir, "Demonstration of lightweight gamma spectromety systems in urban environments," J. Environ. Radioact., Vol.124, pp. 22-28, 2013. https://doi.org/10.1016/j.jenvrad.2013.03.006

[16] M. Andoh, H. Yamamoto, T. Kanno, and K. Saito, "Measurement of ambient dose equivalent rates by walk survey around Fukushima Dai-ichi Nuclear Power Plant Using KURAMA-II until 2016," J. Environ. Radioact., Vols.190-191, pp. 111-121, 2018. https://doi.org/10.1016/j.jenvrad.2018.04.025

[17] P. G. Martin, D. Connor, O. D. Payton, M. Leal-Olloqui, A. C. Keatley, and T. B. Scott, "Development and validation of a high-resolution mapping platform to aid in the public awareness of radiological hazards," J. Radiol. Prot., Vol.38, No.1, pp. 329-342, 2018. https://doi.org/10.1088/1361-6498/aaa914

[18] W. Poltabtim, S. Musikawan, A. Thumwong, Y. Omori, C. Kranrod, M. Hosoda, K. Saenboonruang, and S. Tokonami, "Estimation of Ambient Dose Equivalent Rate Distribution Map Using Walking Survey Technique in Hirosaki City, Aomori, Japan," Int. J. Environ. Res. Publ. Health, Vol.20, No.3, Article No.2657, 2023. https://doi.org/10.3390/ijerph20032657

[19] Group for Fukushima Mapping Project, "Investigations on Distribution of Radioactive Substances Owing to the Fukushima Daiichi Nuclear Power Station Accident in the Fiscal Year 2020 (Contact Research)," JAEA-Technology, 2021-025, 2022 (in Japanese). https://doi.org/10.11484/jaea-technology-2021-025

[20] Y. Sanada, Y. Urabe, M. Sasaki, K. Ochi, and T. Torii, "Evaluation of ecological half-life of dose rate based on airborne radiation monitoring following the Fukushima Dai-ichi nuclear power plant accident," J. Environ. Radioact., Vol.192, pp. 417-425, 2018. https://doi.org/10.1016/j.jenvrad.2018.07.016

[21] S. Mikami, T. Maeyama, Y. Hoshide, R. Sakamoto, S. Sato, N. Okuda, T. Sato, H. Takemiya, and K. Saito, "The air dose rate around the Fukushima Dai-ichi Nuclear Power Plant: Its spatial characteristics and temporal changes until December 2012," J. Environ. Radioact., Vol.139, pp. 250-259, 2015. https://doi.org/10.1016/j.jenvrad.2014.08.020

[22] Institut de Radioprotection et de Sûreté Nucléaire. https://sfrp.asso.fr/blog/les-manifestations/fukushima-10-ans-apres/ [Accessed March 14, 2024]

[23] G. Steinhauser, A. Brandl, and T. E. Johnson, "Comparison of the Chernobyl and Fukushima nuclear accidents: A review of the environmental impacts," Sci. Tot. Environ., Vol.470-471, pp. 800-817, 2014. https://doi.org/10.1016/j.scitotenv.2013.10.029

[24] International Atomic Energy Agency, "Calibration of Radiation Protection Monitoring Instruments," Safety Reports Series, No.16, 2000. https://www-pub.iaea.org/MTCD/Publications/PDF/P074_scr.pdf [Accessed March 12, 2024]

[25] International Atomic Energy Agency, "Guidelines for Radioelement Mapping Using Gamma Ray Spectrometry Data," IAEA, IAEA-TECDOC-1363, 2003. https://www-pub.iaea.org/MTCD/Publications/PDF/te_1363_web.pdf [Accessed March 12, 2024]

[26] B. Lauritzen, D. W. Sandarson, A. Crosswell, M. Scott, R. Finck, and S. Karlsson, "ECOMAGS: Initial results from the RESUME 2002 Exercise," NKS, NKS-86, 2002. https://inis.iaea.org/collection/NCLCollectionStore/_Public/34/057/34057813.pdf [Accessed March 12, 2024]

[27] D. C. W. Sandarson, A. J. Crosswell, I. M. Anthony, and S. Murphy, "Report on SURRC Participation in the ECCOMAGS Project Resume 2002 Exercise," Scottish Universities Research and Reactor Centre, 2002. https://eprints.gla.ac.uk/39226/1/39226.pdf [Accessed March 12, 2024]

[28] D. C. W. Sandarson, A. J. Crosswell, E. M. Scott, and J. J. Lang, "Demonstrating the European capability for airborne gamma spectrometry: Results from the ECOMAGES exercise," Rad. Prot. Dos., Vol.109, Nos.1-2, pp. 119-125, 2004. https://doi.org/10.1093/rpd/nch243

[29] B.-J. Kim, M. Sasaki, and Y. Sanada, "Comparison of the Fukushima radioactive mapping by two different airborne radiation monitoring system," Prog. Nucl. Sci. Technol., Vol.6, pp. 130-133, 2019. https://doi.org/10.15669/pnst.6.130

[30] Y.-Y. Ji, K. Ochi, S. B. Hong, S. Nakama, Y. Sanada, and S. Mikami, "Performance of in situ gamma-ray spectrometry in the assessment of radioactive cesium deposition around the Fukushima Daiichi nuclear power plant," Rad. Phys. Chem., Vol.179, Article No.109205, 2021. https://doi.org/10.1016/j.radphyschem.2020.109205

[31] K. Ochi, M. Sasaki, M. Ishida, and Y. Sanada, "Comparison of airborne and ground-based tools for used for radiation measurement in the environment," Prog. Nucl. Sci. Technol., Vol.6, pp. 103-107, 2019. https://doi.org/10.15669/pnst.6.103

[32] Y. Sanada, M. Ishida, K. Yoshimura, and S. Mikami, "Comparison of Dose Rates from Four Surveys around the Fukushima Daiichi Nuclear Power Plant for Location Factor Evaluation," J. Rad. Prot. Res., Vol.46, No.4, pp. 184-193, 2021. https://doi.org/10.14407/jrpr.2021.00171

[33] Geospatial Information Authority of Japan, "Latest national pictures (seamless)." https://www.gsi.go.jp/ENGLISH/index.html [Accessed February 27, 2023]

[34] H. Kato, Y. Onda, X. Gao, Y. Sanada, and K. Saito, "Reconstruction of a Fukushima accident-derived radiocesium fallout map for environmental transfer studies," J. Environ. Radioact., Vol.210, Article No.105996, 2019. https://doi.org/10.1016/j.jenvrad.2019.105996

[35] Y. Sanada, K. Yoshimura, Y. Urabe, T. Iwai, and E. W. Katengeza, "Distribution map of natural gamma-ray dose rates for studies of the additional exposure dose after the Fukushima Dai-ichi Nuclear Power Station accident," J. Environ. Radioact., Vols.223-224, Article No.106397, 2020. https://doi.org/10.1016/j.jenvrad.2020.106397

[36] S. Tsuda, T. Yoshida, M. Tsutsumi, and K. Saito, "Characteristics and verification of a carborne survey system for dose rates in air: KURAMA-II," J. Environ. Radioact., Vol.139, pp. 260-265, 2015. https://doi.org/10.1016/j.jenvrad.2014.02.028

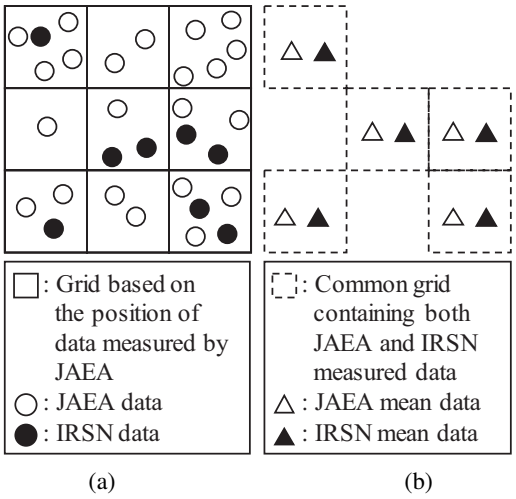

Fig. 13. Establishment of the grid used to calculate the average air dose rate. (a) Creation of the grid based on the location information of JAEA's measurement data and (b) extraction of the common grid of the measured data of both JAEA and IRSN.

[37] United Nations Scientific Committee on the Effects of Atomic Radiation, "Levels and effects of radiation exposure due to the accident at the Fukushima Daiichi Nuclear Power Station: Implications of information published since the UNSCEAR 2013 Report," UNSCEAR 2020/2021 Report, United Nations, 2022. https://www.unscear.org/docs/publications/2020/UNSCEAR_2020_21_Report_Vol.II.pdf [Accessed March 12, 2024]

[38] P. Bossew, G. Cinelli, M. Hernández-Ceballos, N. Cernohlawek, V. Gruber, B. Dehandschutter, F. Menneson, M. Bleher, U. Stöhlker, I. Hellmann, F. Weiler, T. Tollefsen, P. V. Tognoli, and M. de Cort, "Estimating the terrestrial gamma dose rate by decomposition of the ambient dose equivalent rate," J. Environ. Radioact., Vol.166, pp. 296-308, 2017. https://doi.org/10.1016/j.jenvrad.2016.02.013

[39] E. Buchanan, A. J. Cresswell, B. Seitz, and D. C. W. Sanderson, "Operator related attenuation effects in radiometric surveys," Radiation Measurements, Vol.86, pp. 24-31, 2016. https://doi.org/10.1016/j.radmeas.2015.12.029

[40] V. Ramzaev, C. Bernhardsson, A. Barkovsky, I. Romanovich, J. Jarneborn, S. Mattsson, A. Dvornik, and S. Gaponenko, "A backpack γ-spectrometer for measurements of ambient dose equivalent rate, $\dot{H}^*(10)$, from ^{137}Cs and from naturally occurring radiation: The importance of operator related attenuation," Radiation Measurements, Vol.107, pp. 14-22, 2017. https://doi.org/10.1016/j.radmeas.2017.10.002

Appendix A. Supplementary Information (Creation of Common Grid)

A square grid was created using ArcGIS (Environmental Systems Research Institute Inc., California, USA) based on the location information of the air dose rate measurement data the JAEA obtained (**Fig. 13(a)**). A grid was maintained if it contained at least one IRSN measurement point and one JAEA measurement point. The average air dose rate for each grid was calculated for each organization (**Fig. 13(b)**). The horizontal positioning accuracy of the GNSS unit associated with the detector was evaluated to determine the grid size (**Table 4**). We used the root mean square (RMS) as an evaluation metric, which is the radius of the circle containing 63%–68% of all data relative to the reference coordinates.

The same detectors and GNSS units were used for the

Table 4. Information about the GNSS unit's horizontal position accuracy.

Organization	**JAEA**					**IRSN**				
Survey	Manborne		Carborne		Airborne	Manborne		Carborne		Airborne
Site	A	B	A	B	A	A	B	A	B	A
n	103	122	104	161	614	–	–	–	–	594
Calculated RMS [cm]	21	48	2.6	7.3	51	–	–	–	–	160
Reference RMS [cm]	30		30		40	30		30		30

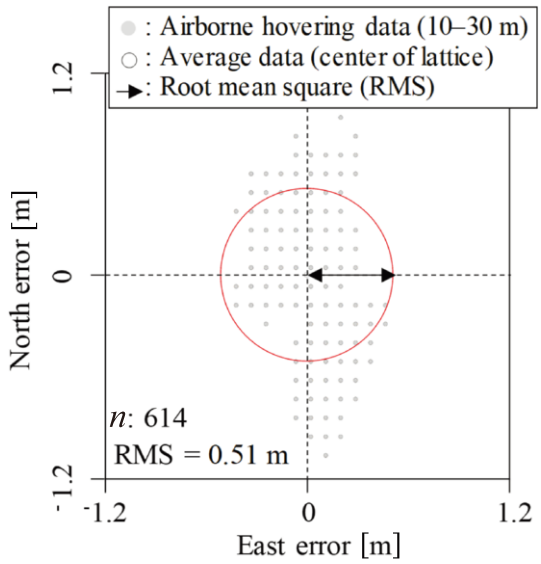

Fig. 14. Example of the evaluation horizontal position accuracy based on the airborne survey results obtained by JAEA.

manborne and carborne surveys. The location information measured outside the car was used to evaluate the RMS of the manborne survey, whereas that measured inside the car was used to evaluate the RMS of the carborne survey.

For the airborne survey, a grid was created based on position information from the JAEA flight at 30 m agl. The RMS was calculated using position information measured at ground altitudes of 10 m, 20 m, and 30 m during hovering flights.

Figure 14 shows an image of RMS evaluation for the JAEA's airborne survey. The RMS evaluated according to the data from each field survey was almost equivalent to the RMS of the catalog specifications proposed by the manufacturer (**Table 4**).

Considering these RMS values, the integration interval of the counts shown in **Table 2**, and the movement speed shown in **Table 3**, the grid size was set to maximize the data contained in each grid. The length of one side of the square grid was defined as 5 m for the manborne and airborne surveys and 50 m for the carborne survey.

Appendix B. Supplementary Information (Dose Rate Evaluation)

Equations (5)–(10) show the calculation of the dose rates in Eq. (2).

$$D_{1\mathrm{m}} = D_{\mathrm{L}} + D_{\mathrm{Cos}} + D_{\mathrm{Rad}} + D_{\mathrm{BG}}, \quad (5)$$

$$D_{\mathrm{L}} = D_{\mathrm{L},\mathrm{H_{Alt}}} H_{\mathrm{m,p}}, \quad (6)$$

$$D_{\mathrm{L},\mathrm{H_{Alt}}} = D_{\mathrm{Det},\mathrm{H_{Alt}}} - D_{\mathrm{Cos},\mathrm{H_{Alt}}} MF_{\mathrm{Cos}} - D_{\mathrm{Rad}} - D_{\mathrm{BG}}, \quad (7)$$

$$D_{\mathrm{Cos}} = D_{\mathrm{Cos},\mathrm{H_{Alt}}} \exp\left[-H_{\mathrm{std}} AF_{\mathrm{Cos}}\right], \quad (8)$$

$$D_{\mathrm{Cos},\mathrm{H_{Alt}}} = D_{\mathrm{Cos},\mathrm{H_s}} \exp\left[H_{\mathrm{Alt}} AF_{\mathrm{Cos}}\right], \quad (9)$$

$$H_{\mathrm{m,p}} = \exp\left[\left\{\frac{T_{\mathrm{std}} P_{\mathrm{m}} H_{\mathrm{Alt}}}{(T_{\mathrm{m}} + T_{\mathrm{std}}) P_{\mathrm{std}}} - H_{\mathrm{std}}\right\} AF_{\mathrm{Air}}\right], \quad (10)$$

where $D_{1\mathrm{m}}$ is the air dose rate at the standard 1 m altitude (H_{std} [m]) [μSv/h], D_{L} is the local air dose rate without a natural dose rate contribution at H_{std} [μSv/h], D_{Cos} is the air dose rate derived from cosmic rays at H_{std} [μSv/h], D_{Rad} is the air dose rate derived from radon progeny at H_{std} [μSv/h], D_{BG} is the background air dose rate derived from self-contamination of a detector [μSv/h], $D_{\mathrm{L},\mathrm{H_{Alt}}}$ is the local air dose rate at flight altitude (H_{Alt} [m]) [μSv/h], $H_{\mathrm{m,p}}$ is the factor of the altitude corrected for the temperature and atmospheric pressure [m], $D_{\mathrm{Det},\mathrm{H_{Alt}}}$ is the air dose rate at H_{Alt} calculated in Eq. (1) [μSv/h], $D_{\mathrm{Cos},\mathrm{H_{Alt}}}$ is the local air dose rate derived from cosmic rays at H_{Alt} [μSv/h], MF_{Cos} is the measured cosmic factor, AF_{Cos} is the cosmic attenuation factor [/m], $D_{\mathrm{Cos},\mathrm{H_s}}$ is the air dose rate derived from cosmic rays at sea level (H_{s} [m]) [μSv/h], T_{std} is the standard temperature (273 K), P_{m} is the measured pressure [hPa], T_{m} is the measured temperature [K], P_{std} is the standard pressure (1013 hPa), and AF_{Air} is the air attenuation factor [/m]. The first data treatment was performed using default data as follows: AF_{Cos} = 438.8/m, AF_{Air} = 0.0056/m, $D_{\mathrm{Cos,Hs}}$ = 32 nSv/h, MF_{Cos} = 0.075, D_{Rad} = 0 nSv/h (considered negligible), and D_{BG} = 2 nSv/h (considered negligible).

Name:
Kotaro Ochi

ORCID:
0000-0002-3753-9718

Affiliation:
Research Engineer, Sector of Fukushima Research and Development, Collaborative Laboratories for Advanced Decommissioning Science, Japan Atomic Energy Agency

Address:
45-169 Sukakeba, Kaibama-aza, Haramachi-ku, Minamisoma, Fukushima 975-0036, Japan

Brief Career:
2016- Sector of Fukushima Research and Development, Japan Atomic Energy Agency
2023 Received Ph.D. degree from Graduate School of Frontier Sciences, The University of Tokyo

Selected Publications:
• K. Ochi et al., "Validation study of ambient dose equivalent conversion coefficients for radiocaesium distributed in the ground: Lessons from the Fukushima Daiichi Nuclear Power Station accident," Rad. Environ. Biophys., Vol.61, pp. 147-159, 2022. https://doi.org/10.1007/s00411-022-00969-3
• K. Ochi et al., "Comparison of airborne and ground-based tools used for radiation measurement in the environment," Prog. Nucl. Sci. Technol., Vol.6, pp. 103-107, 2019. https://doi.org/10.15669/pnst.6.103

Academic Societies & Scientific Organizations:
• Atomic Energy Society of Japan (AESJ)
• Japan Health Physics Society (JHPS)

Name:
Evelyne Barker

ORCID:
0000-0001-8035-5618

Affiliation:
Project Manager, Environment Division, Institute for Radiation Protection and Nuclear Safety

Address:
31 avenue de la division Leclerc, Fontenay-aux-Roses 92260, France

Brief Career:
1998- Laboratory of Gamma Spectrometry Measurement of Environmental Samples, Institute for Radiation Protection and Nuclear Safety
2017- Project Manager in polluted sites characterization, Institute for Radiation Protection and Nuclear Safety

Selected Publications:
• E. Barker et al., "Summing spectra in gamma spectrometry for improving detection of low-level radionuclides in aerosol samples," Radioprotection, Vol.40, No.Suppl. 1, pp. S733-S737, 2005. https://doi.org/10.1051/radiopro:2005s1-107
• E. Barker et al., "Determination of ^{226}Ra in solid samples of few milligrams after mineralization and measurement by solid scintillation," J. Radioanal. Nucl. Chem., Vol.314, pp. 353-358, 2017. https://doi.org/10.1007/s10967-017-5399-3
• A. Gourgiotis, T. Ducasse, E. Barker et al., "Silicon isotope ratio measurements by inductively coupled plasma tandem mass spectrometry for alteration studies of nuclear waste glasses," Analytica Chimica Acta, Vol.954, pp. 68-76, 2017. https://doi.org/10.1016/j.aca.2016.11.063

Name:
Shigeo Nakama

ORCID:
0000-0003-2386-7419

Affiliation:
Assistant Principal Engineer, Sector of Fukushima Research and Development, Collaborative Laboratories for Advanced Decommissioning Science, Japan Atomic Energy Agency

Address:
45-169 Sukakeba, Kaibama-aza, Haramachi-ku, Minamisoma, Fukushima 975-0036, Japan

Brief Career:
2000- Japan Nuclear Cycle Development Institute
2005- Japan Atomic Energy Agency
2012- Sector of Fukushima Research and Development, Japan Atomic Energy Agency

Selected Publications:
• S. Nakama et al., "Temporal decrease in air dose rate in the sub-urban area affected by the Fukushima Dai-ichi Nuclear Power Plant accident during four years after decontamination works," J. Environ. Radioact., Vols.208-209, Article No.106013, 2019. https://doi.org/10.1016/j.jenvrad.2019.106013
• K. Yoshimura, S. Nakama, and K. Fujiwara, "Radiation Monitoring in the Residential Environment: Time Dependencies of Air Dose Rate and ^{137}Cs inventory," J. Rad. Prot. Res., Vol.47, No.1, pp. 30-38, 2022. https://doi.org/10.14407/jrpr.2021.00199

Academic Societies & Scientific Organizations:
• Atomic Energy Society of Japan (AESJ)
• Japan Society of Civil Engineers (JSCE)
• The Minig and Materials Processing Institute of Japan (MMIJ)
• Japanese Society of Rock Mechanics (JSRM)

Name:
Marc Gleizes

Affiliation:
Director, Environment Division, Institute for Radiation Protection and Nuclear Safety

Address:
31 avenue de la division Leclerc, Fontenay-aux-Roses 92260, France

Brief Career:
1996- Institute for Radiation Protection and Nuclear Safety
2006- Head, Department of Non-Proliferation, Nuclear Measurement, Radiological Environment Monitoring, Institute for Radiation Protection and Nuclear Safety
2019- Deputy Director, Environmental Department, Institute for Radiation Protection and Nuclear Safety
2023- Director, Environmental Department, Institute for Radiation Protection and Nuclear Safety

Selected Publications:
• A. Habibi, B. Boulet, M. Gleizes et al., "Rapid determination of actinides and ^{90}Sr in river water," Analytica Chimica Acta, Vol.883, pp. 109-116, 2015. https://doi.org/10.1016/j.aca.2015.04.025

Academic Societies & Scientific Organizations:
• French Radioprotection Society (SFRP)

Name:
Erwan Manach

Affiliation:
Deputy Head, Remote Sensing Laboratory, Environment Division, Institute for Radiation Protection and Nuclear Safety

Address:
31 avenue de la division Leclerc, Fontenay-aux-Roses 92260, France

Brief Career:
2005- Project Manager, Clinical Research Department, French National Cancer Institute
2010- Environmental Radioactivity Engineer, Institute for Radiation Protection and Nuclear Safety

Selected Publications:
• E. Manach and O. Gal, "Experimental and simulation results of gamma imaging with hybrid pixel detectors," Nucl. Instr. and Meth., Vol.531, Nos.1-2, pp. 38-51, 2004. https://doi.org/10.1016/j.nima.2004.05.072
• E. Manach et al., "How to improve patients and investigators' information on clinical trials: The example of French registry for clinical trials in oncology," J. of Clinical Oncology, Vol.26, No.15_suppl, Article No.17555, 2008. https://doi.org/10.1200/jco.2008.26.15_suppl.17555
• M.-A. Gonze, C. Mourlon, P. Calmon, E. Manach, C. Debayle, and J. Baccou, "Modelling the dynamics of ambient dose rates induced by radiocaesium in the Fukushima terrestrial environment," J. of Environmental Radioactivity, Vol.161, pp. 22-34, 2016. https://doi.org/10.1016/j.jenvrad.2015.06.003

Academic Societies & Scientific Organizations:
• French Radioprotection Society (SFRP)
• European Radiation Dosimetry Group (EURADOS), WG3 Environmental Dosimetry

Name:
Vincent Faure

Affiliation:
Radioprotection Engineer, Environment Division, Institute for Radiation Protection and Nuclear Safety

Address:
31 avenue de la division Leclerc, Fontenay-aux-Roses 92260, France

Brief Career:
2005- Agence Nationale pour la gestion des Déchets Radioactifs
2017- Institute for Radiation Protection and Nuclear Safety

Name:
Yukihisa Sanada

ORCID:
0000-0002-5388-2444

Affiliation:
Senior Principal Engineer, Sector of Fukushima Research and Development, Collaborative Laboratories for Advanced Decommissioning Science, Japan Atomic Energy Agency

Address:
45-169 Sukakeba, Kaibama-aza, Haramachi-ku, Minamisoma, Fukushima 975-0036, Japan

Brief Career:
2000- Japan Nuclear Cycle Development Institute
2005- Japan Atomic Energy Agency
2006 Received Ph.D. degree from Graduate School of Science and Technology, Niigata University
2011- Sector of Fukushima Research and Development, Japan Atomic Energy Agency

Selected Publications:
• Y. Sanada et al., "External exposure assessment in the Fukushima accident area for governmental policy planning in Japan: Part 1. Methodologies for personal dosimetry applied after the accident," J. Rad. Res., Vol.64, No.1, pp. 2-10, 2023. https://doi.org/10.1093/jrr/rrac079
• Y. Sanada et al., "Basic study on tritium monitor using plastic scintillator for treated water discharge at Fukushima Daiichi Nuclear Power plant," J. Nucl. Sci. Technol., pp. 1-10, 2023. https://doi.org/10.1080/00223131.2023.2258880

Academic Societies & Scientific Organizations:
• Atomic Energy Society of Japan (AESJ)